Available online at www.sciencedirect.com
SCIENCE DIRECT
Journal of Catalysis 235 (2005) 403–412
JOURNAL OF CATALYSIS
www.elsevier.com/locate/jcat

Hydrodesulfurization of dibenzothiophene and 4,6-dimethyl-dibenzothiophene: Gallium effect over NiMo/Al_2O_3 sulfided catalysts

Efraín Altamirano [a,b], José Antonio de los Reyes [a,*], Florentino Murrieta [c], Michel Vrinat [b]

[a] *Universidad A. Metropolitana-Iztapalapa, Área de Ingeniería Química, Av. FFCC R. Atlixco No. 186, Col. Vicentina, Iztapalapa, 09340 México, DF, Mexico*
[b] *Institut de Recherches sur la Catalyse, 2 Av. A. Einstein, 69626 Villeurbanne cedex, France*
[c] *Instituto Mexicano del Petróleo, Eje central Lázaro Cárdenas 152, 07730 México, DF, Mexico*

Received 3 June 2005; revised 31 August 2005; accepted 5 September 2005

Abstract

The influence of gallium on alumina-supported NiMo catalysts was investigated by correlating their physicochemical properties with the hydrodesulfurization (HDS) activity of model molecules. The Ga–γ-Al_2O_3 supports were prepared by impregnation of Ga (0.6–5.9 wt%) on γ-Al_2O_3. The NiMo catalysts were prepared following the same method on calcined Ga–Al_2O_3. The N_2-physisorption results showed that Ga did not affect the textural properties of both γ-Al_2O_3 and NiMo/γ-Al_2O_3. When the Ga–Al_2O_3 supports were calcined at 723 K all Ga ions presented a high dispersion, forming a different structure than that observed in bulk Ga_2O_3. The XPS and the TPR-S showed that the Ga addition modified the structural properties of NiMo depending on the amount of Ga. In the HDS of DBT and 4,6-DMDBT, the Ga–Al_2O_3 supported NiMo catalysts at loadings of Ga below to 1.2 wt% showed higher activity than that of a NiMo/Al_2O_3 sample.

Keywords: Ga_2O_3; Ga_2S_3; Al_2O_3; NiMo; Hydrodesulfurization; Dibenzothiophene; 4,6-Dimethyl-dibenzothiophene; XPS; TPR

1. Introduction

The current environmental regulations that impose very low sulfur content in diesel cuts have spurred research on hydrotreating catalysts. The commercial HDS catalysts consist of an active phase of molybdenum (Mo) promoted by nickel (Ni) or cobalt (Co) usually supported on alumina. Nevertheless, it has been recognized since the very first studies related to these solids (CoMo or NiMo/Al_2O_3) that alumina is not an inert carrier. On one hand, the promoter ion (Co or Ni) can react with the support and occupy octahedral or tetrahedral sites in external layers or even form an inactive phase such as $CoAl_2O_4$ ($NiAl_2O_4$) depending on the preparation conditions [1]. On the other hand, the molybdates interact strongly with the support from the first steps of catalyst preparation through Mo–O–Al anchors [2,3]. Topsøe and Topsøe [4] and many other authors have suggested that the improvement of HDS catalysts is closely related to the formation of the so-called "NiMoS" (CoMoS) phase. Thus the amount of the NiMoS phase should be increased by reducing the concentration of inactive species to improve the performance of HDS catalysts. As pointed out by several authors, the carrier plays a fundamental role, because strong interactions prevent NiMoS phase formation. Addition of a third metal as an additive may also influence the speciation of Ni and Mo and, consequently, HDS activity. Along this line, many papers have reported the influence of additives or modifiers, such as Mg [5–9], Ca [6,8,9], Ti [8], Fe [8], Mn [9] and Zn [5,10–13]. Unfortunately, the reports on the effects of these additives are rather conflicting. Martinez and Mitchell [5] showed that adding small amounts of Mg to CoMo/Al_2O_3 catalysts resulted in increased HDS activity, whereas adding large amounts of Mg resulted in decreased HDS activity. Muralidhar et al. [6] reported that adding 5% of Ca or Mg before or after Mo and Co impregnation decreased HDS activity. Hercules et al. [7] reported that Mg forms spinel-type species ($MgAl_2O_4$)

* Corresponding author.
E-mail address: jarh@xanum.uam.mx (J.A. de los Reyes).

0021-9517/$ – see front matter
doi:10.1016/j.jcat.2005.09.011

or free oxides on the alumina surface, promoting Mo or W dispersion, and Saini et al. [8] reported that Ca cannot easily form $CaAl_2O_4$ species due to its larger ionic radius compared with Mg (Mg^{2+}, 0.66; Ca^{2+}, 0.94). Transition metals (Me = Ti, Fe, or Mn) as additives scarcely form $MeAl_2O_4$ species and have poor dispersion when they are impregnated on alumina and calcined around 773 K; therefore, these metals are not suitable for use in improving HDS activity. Martinez [5] showed that adding small amounts of Zn to the $CoMo/Al_2O_3$ resulted in increased HDS activity, depending on the sequence of impregnation and on the calcination temperatures, in agreement with findings of other authors [11].

Gallium has been scarcely studied as an additive of HDT catalysts. However, some papers have been devoted to the characterization of Ga as an additive in alumina-supported $CoMo/Al_2O_3$ and $NiMo/Al_2O_3$ catalysts. In early works, Cimino et al. [10] and Lo Jacono et al. [14] observed a high affinity of Ga^{3+} to the tetrahedral sites of alumina, modifying the ratio of tetrahedral/octahedral species of Ni ($Ni^{2+}_{tet}/Ni^{2+}_{oct}$) in the Ni/Al_2O_3 solid. A similar effect was observed when gallium was added to the CoMo catalyst, and these authors observed that the $Co^{2+}_{tet}/Co^{2+}_{oct}$ ratio changed as a function of the metal loading (Ga, Co, and Mo) and of the impregnation sequence. As far as we know, these catalysts were not tested in HDS reactions; therefore, in this context, our experimental goals are aimed at investigating the additive effect of gallium. Indeed, recent results reported a positive effect of Ga as a second promoter to a NiMo catalyst in the pyridine hydrodenitrogenation (HDN) [15], and mixed gallium/aluminum oxides have been used as support for CoMo catalysts in the HDS of thiophene [16]. In this paper we report the study of a series of $NiMo/Ga–Al_2O_3$ catalysts with a gallium content ranging from 0 to 5.9 wt%. These catalysts were tested in the HDS of dibenzothiophene and 4,6-dimethyl-dibenzothiophene, and a discussion of these results considering the characterization in the sulfided state by X-ray diffraction (XRD), X-ray photoelectron spectroscopy (XPS), and temperature-programmed reduction on the sulfided samples (TPR-S) is presented.

2. Experimental

2.1. Catalyst preparation

The supports were prepared by pore-filling impregnation of a commercial γ-Al_2O_3 (high purity; BET surface area, 240 $m^2\,g^{-1}$; pore volume (V_p), 0.63 $cm^3\,g^{-1}$; particle size, 80–100 μm) with an aqueous solution of $Ga(NO_3)_3 \cdot xH_2O$ (Aldrich Chemical) at constant pH of 5.4 to obtain supports with 0, 0.6, 1.2, 1.8, 2.9, and 5.9 wt% of metal. After 12 h, the obtained solids were dried at 393 K for 12 h and calcined at 723 K for 4 h under a flow of air (5.16×10^{-3} mol min^{-1}) with a heating rate of 1 K min^{-1}.

NiMo catalysts were prepared by the pore-filling method on calcined Ga_2O_3/γ-Al_2O_3 samples ($Ga–Al_2O_3$) with aqueous solutions of ammonium heptamolybdate [AHM, $(NH_4)_6Mo_7O_{24} \cdot 4H_2O$; Merck] and nickel nitrate [$Ni(NO_3)_2 \cdot 6H_2O$; Aldrich Chemical]. The loading of the metals was estimated per nm^2 of initial surface area of alumina. For the molybdenum and nickel 2.8 and 1.2 at nm^{-2} were added, respectively, leading to an atomic Ni $r = 0.3$, with $r = Ni/(Ni + Mo)$.

In a typical preparation, first a solution of AHM was prepared and the pH was adjusted to 8 by adding a basic solution (NH_4OH, Baker). Then, the support was impregnated and after 12 h, the solids were dried under a stream of air (5.16×10^{-3} mol min^{-1}) at 393 K for 12 h, with a heating rate of 3 K min^{-1}. The impregnation of nickel was performed with a solution of nickel nitrate at constant pH of 5.4. After 12 h, the obtained solids were dried at 393 K for 720 min and calcined at 673 K for 4 h under a stream of air (5.16×10^{-3} mol min^{-1}) with a heating rate of 1 K min^{-1}.

The oxide phases (mass of sample ca. 1 g) were sulfided at 673 K for 2 h with a mixture of H_2S/H_2 (15% H_2S) at a total flow rate of 2.97×10^{-3} mol min^{-1} and a heating rate of 5 K min^{-1}. After this step, the catalysts were cooled to room temperature and flushed with N_2 for about 30 min and kept in sealed bottles under argon.

2.2. Characterization techniques

After the final calcination, the metal contents were determined by atomic absorption after appropriate dissolution of the solids samples; the results are presented in Table 1. This table also gives the nomenclature and specification of all of the catalysts. Elemental sulfur analyses were performed after combustion at 1623 K in a CS-mat 5500 instrument (Ströhlein). The emitted amounts of SO_2 were analyzed by infrared spectroscopy.

Surface area, pore volume, and pore size distribution were obtained from N_2 adsorption and desorption isotherms using the conventional BET and BJH methods. The samples were first dried at 393 K for 2 h and subsequently outgassed at 573 K under vacuum. Then N_2 adsorption measurements were carried out at 73 K.

The XRD patterns of the calcined and sulfided catalysts were recorded on a Bruker D5005 diffractometer using Cu-K_α radiation (0.154184 nm) at 3–80° with a 0.02° step size and 1 s at every step.

XPS measurements were performed on a VG Instrument type ESCALAB 200R spectrometer equipped with an Al-K_α source ($h\nu = 1486.6$ eV). The shifts of the peak core line due to the charge of the sample were corrected by taking the Al-2p line of the catalyst support, γ-Al_2O_3 (Al 2p, 74.0 eV) as a reference. For the XPS measurements, the presulfided powder sample was introduced into an argon-filled glove box and pressed on indium foil fixed on the sample holder under the protection of inert Ar atmosphere. The sample holder was then transferred into the preparation chamber of the XPS equipment and passed into the analysis chamber after evacuation overnight (10^{-9} Pa). The XPS spectrum corresponds to the plot of the variation in the numbers of emitted electrons versus their kinetic energy values, that is, their binding energy values.

In the TPR-S experiments, an appropriate amount of the sulfided sample (50 mg) was maintained between two layers of quartz wool in a U-shaped quartz tube reactor with an outside

Table 1
Textural properties, chemical analysis and nomenclature of prepared catalysts.

Support	Catalyst	N_2 adsorption measurements			Metal content (wt%)		
		A_{BET}	V_p	d_p	Ga	Ni	Mo
γ-Al_2O_3	NiMo	213	0.55	100	0.00	2.43	8.64
0.6Ga–Al_2O_3	0.6NiMo	218	0.49	102	0.61	2.32	8.47
1.2Ga–Al_2O_3	1.2NiMo	220	0.50	100	1.20	2.34	8.46
1.8Ga–Al_2O_3	1.8NiMo	219	0.52	100	1.74	2.35	8.41
2.9Ga–Al_2O_3	2.9NiMo	215	0.43	98	2.86	2.30	8.41
5.9Ga–Al_2O_3	5.9NiMo	196	0.44	96	5.91	2.34	8.34

A_{BET}, surface area ($m^2\,g^{-1}$); V_p, pore volume ($ml\,g^{-1}$); and d_p, pore diameter (Å).

diameter of 6 mm and inside diameter of 4 mm. The quantity of H_2S was measured by a photoionization detector (PID) (type PI 52-02A; HNU Systems). The energy of the lamp was 10.2 eV, approaching the amount needed for the ionization of H_2S. Before the reduction step, the detector was calibrated with a standardized gas mixture of 500 ppm H_2S/Ar (the exact content of H_2S with a relative precision of 3%). When the PID signal was stabilized, the reactor was switched to purified H_2 (flow rate, 50 $ml\,min^{-1}$) to first purge the rest of H_2S for 10 min; then the sample was reduced at a temperature that was increased linearly up to 1323 K at a rate of 4 $K\,min^{-1}$). The composition of the outlet gas mixture was analyzed every minute with an automated sampling valve. The amount of H_2S was calculated according to previous studies [17,18].

2.3. Catalytic activity tests

The HDS of DBT (Aldrich; 99.9%) was carried out in a continuous-flow microreactor in the vapor phase working with a total flow of 6 $l\,h^{-1}$, $p_{H_2} = 4$ MPa, $p_{DBT} = 2.4$ kPa, and $p_{H_2S} = 5.2$ kPa, at 513–533 K. The catalyst mass was approximately 50 mg. The products were analyzed by gas chromatography (GC).

The HDS of 4,6-DMDBT was carried out in a three-phase continuous-flow microreactor with dodecane as the solvent, working with a total mass liquid flow of 3.8 $g\,h^{-1}$, $p_{H_2} =$ 3 MPa, and H_2 flow = 0.026 $l\,min^{-1}$, at three different temperatures (553, 573, and 593 K). The catalyst mass was approximately 50 mg. The products were analyzed by GC.

The specific reaction rates were calculated according to the following expression:

$$r = \frac{F}{m}(Conv_{DBT}), \tag{1}$$

where r is the specific rate of disappearance of DBT or 4,6-DMDBT ($mol\,g^{-1}\,s^{-1}$), F is the molar flow rate of the reactant ($mol\,s^{-1}$), $Conv_{DBT}$ is the conversion of DBT or 4,6-DMDBT, and m is the catalyst mass (g). All rates were estimated at low conversion (<15%).

Additional experiments were performed in batch mode to assess the evolution with time of the selectivities in the HDS of 4,6-DMDBT. This reaction was performed in a 300-ml batch reactor, magnetically stirred (1000 rpm) (Parr Instruments), equipped with four baffles on the wall to prevent vortex formation. The test conditions were a temperature of 593 K under a hydrogen atmosphere of 5 MPa for 8 h, using 500 mg of sulfided catalyst and 1.41×10^{-3} mol of 4,6-DMDBT dissolved in 150 ml of dodecane (Aldrich Chemical), with 1.4×10^{-3} mol of hexadecane (Aldrich Chemical) used as an internal standard (IS) reference for quantitative analysis. The reactor was flushed with nitrogen and heated under stirring to reach the reaction temperature; then hydrogen was introduced ($p_{tot} = 5$ MPa). The reaction time was determined from this moment. The total pressure was controlled constantly during the course of the reaction by adding hydrogen to compensate for its consumption. Samples were periodically collected and analyzed quantitatively by GC. The reactant conversion and the products yields were determined relative to the IS.

3. Results

3.1. N_2 Adsorption measurements

The catalysts with different Ga content demonstrated almost the same values for the surface area (Table 1). However, a slight decrease (ca. 11%) was observed for the sample containing 5.9 wt% Ga. The pore volume (V_p) and the pore diameter (d_p) did not vary significantly for the whole series.

3.2. XRD

In all Ga–Al_2O_3 supports, the diffraction patterns were practically the same as that of alumina, suggesting that gallium is highly dispersed with a particle size <4 nm, in agreement with transmission electron microscopy results published by Nishi et al. [19]. The presence of gallium produced no significant modification of the XRD patterns of all NiMo-containing samples after calcination or sulfidation (patterns not shown here).

3.3. TPR-S analyses

3.3.1. TPR-S of α-Ga_2S_3 and sulfided γ-alumina

The TPR-S pattern of the bulk commercial α-Ga_2S_3 is shown in Fig. 1a. Three large peaks were observed between 800 and 1350 K, indicating a three-step reduction. The quantitative analysis indicated that the α-Ga_2S_3 was reduced in about 74%. Due to the experimental conditions, we could not continue the reduction above 1350 K, although we did plot a confidential interval to complete the reduction pattern (Fig. 1b). Hence we suggest, taking into account literature results [20], proceeding

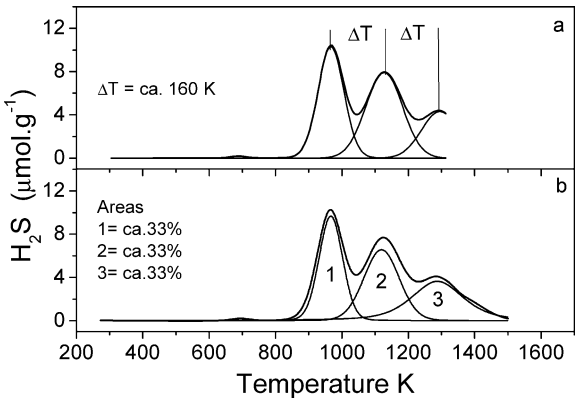

Fig. 1. TPR-S patterns: (a) experimental reduction of commercial sample α-Ga_2S_3 and (b) complete predicted reduction pattern of α-Ga_2S_3.

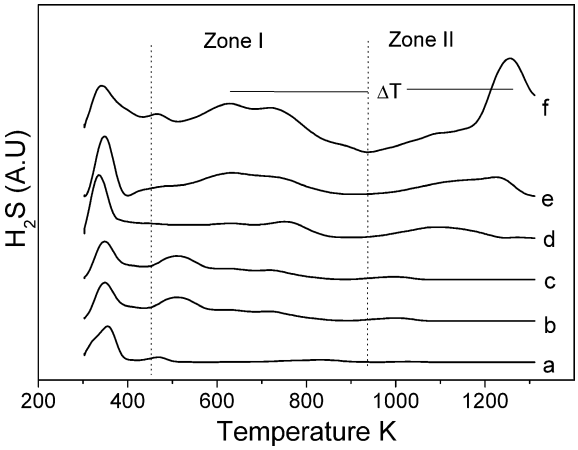

Fig. 2. TPR-S patterns of (a) γ-Al_2O_3, (b) 0.6Ga–Al_2O_3, (c) 1.2Ga–Al_2O_3, (d) 1.8Ga–Al_2O_3, (e) 2.9Ga–Al_2O_3, and (f) 5.9Ga–Al_2O_3. All samples were sulfided at 673 K.

with the reduction of α-Ga_2S_3 as follows:

$$Ga_2S_3 + H_2 \underset{800-1100\ K}{\rightarrow} 2GaS + H_2S, \quad (1)$$

$$2Ga + H_2 \underset{960-1290\ K}{\rightarrow} Ga_2S + H_2S, \quad (2)$$

$$Ga_2S + H_2 \underset{1100-1600\ K}{\rightarrow} Ga^0 + H_2S. \quad (3)$$

In the experimental TPR-S pattern (Fig. 1a), the peak between 800 and 1100 K [step (1)] corresponds to 42% of the total H_2S produced (area under the curve), the peak between 960 and 1290 K [step (2)] represents 42% of the total H_2S, and the peak between 1100 and 1350 K [step (3)] corresponds to 16% of the total H_2S. The temperature difference (ΔT) between each adjacent peak maximum is ca. 160 K.

The quantitative analyses in TPR-S (considering a 10% error) and the elemental sulfur chemical analysis indicate that the H_2S produced in each step is consistent with the stoichiometry of the species involved in the reduction steps. These results led us to consider that the pattern suggested in Fig. 1b (where the H_2S in each step represents 33% of the total H_2S produced) is a helpful approximation to determine the complete Ga_2S_3 reduction.

Table 2
H_2S production in the TPR-S of sulfided supports (Ga–Al_2O_3) and catalysts (0–5.9NiMo)

Support	Zone I[a] (μmol g_{cat}^{-1})	Zone II[a] (μmol g_{cat}^{-1})	Solid	Total (μmol g_{cat}^{-1})
γ-Al_2O_3	0	0	NiMo	1736.58
0.6Ga–Al_2O_3	19.0	0.50	0.6NiMo	1748.30
1.2Ga–Al_2O_3	38.2	3.00	1.2NiMo	1717.89
1.8Ga–Al_2O_3	41.1	24.3	1.8NiMo	1727.26
2.9Ga–Al_2O_3	60.4	55.0	2.9NiMo	1692.25
5.9Ga–Al_2O_3	130	137	5.9NiMo	1696.11
[b]5.9Ga–Al_2O_3	319	355	[c]α-Ga_2S_3	532.30

[a] Data corrected by the extraction of H_2S produced in the alumina TPR-S.
[b] Support sulfided at 873 K.
[c] The mass analyzed correspond to the loading of gallium present in the support 5.9Ga–Al_2O_3.

Fig. 2a shows the TPR-S pattern of the support γ-Al_2O_3 sulfided at 673 K. Production of H_2S was observed between 293 and 400 K, representing the desorbed H_2S. Another zone of H_2S production occurred between 600 and 900 K, corresponding to the reduction of some impurities [21,22] or to the reduction of some elemental sulfur produced by H_2S decomposition during the sulfidation. It has been reported that the reduction of this elemental sulfur can be found only over the support and not over Ni/Al_2O_3, Mo/Al_2O_3, or NiMo/Al_2O_3 solids [23].

3.3.2. *TPR-S of Ga–Al_2O_3 supports*

The TPR-S patterns of Ga–Al_2O_3 supports sulfided at 673 K and with various loadings are shown in Fig. 2b–f. The profiles changed as the amount of gallium was increased. There are two important zones of H_2S production: zone I, in the range of 450–950 K, in which a broad peak increases with the loading of Ga, and zone II (950–1350 K), in which the intensity becomes more significant than that of zone I at a loading over 2.9% of gallium. The total amount of H_2S and the evolution of H_2S in each zone are reported in Table 2. The H_2S desorbed below 450 K was not considered, because this peak was present in all samples.

In Fig. 1, the TPR-S of α-Ga_2S_3 shows a completely different reduction pattern than that of the Ga–Al_2O_3 series (Figs. 2b–f), suggesting that the gallium species on the alumina surface is different than that in the bulk gallium sulfide.

3.3.3. *TPR-S of NiMo catalysts*

Due to the fact that the reduction of gallium sulfide could be superposed to the reduction of the NiMo sulfide phase, we determined, for the sake of simplicity, that all NiMo catalysts could be deconvoluted in the same way. Interpretation of the patterns is based on work by Arnoldy et al. and Mangnus et al. [22,24,25], who classified the H_2S produced during the TPR-S in four types, as described below.

The deconvolution treatment was adjusted to four peaks that correspond to the four types of H_2S sources. For the TPR-S of NiMo (Fig. 3), the first peak appeared between 350 and 500 K with a maximum at 393 K (peak 1). The H_2S produced in this region is assigned mainly to the desorbed H_2S (type 1), and some part could be produced by the hydrogenation of nonstoichiometric sulfur (S_x). Peak 2, between 300 and 900 K with a

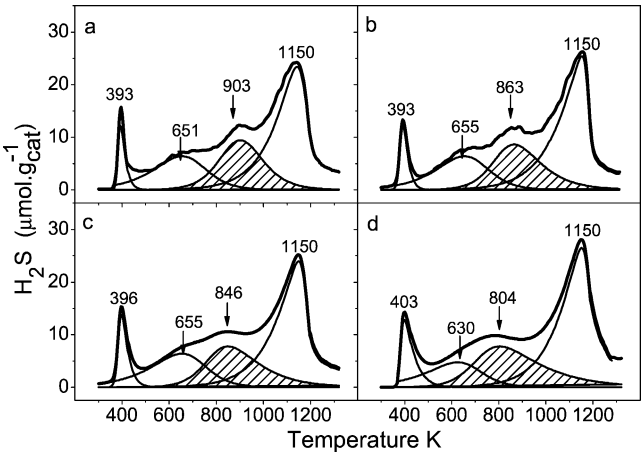

Fig. 3. TPR-S patterns of (a) NiMo, (b) 0.6NiMo, (c) 1.8NiMo and (d) 5.9NiMo catalysts. All catalysts were sulfided at 673 K. Dashed area is assigned to nickel species.

maximum at 651 K, could be assigned to H_2S produced by a recombination of S–H groups, a reaction of H_2 and S–H (type 2), and a reaction that may involve a surface nonstoichiometric sulfur (S_x) anion and H_2, forming H_2S and anion vacancies on the catalyst (type 3) [21,26],

$$\begin{matrix}\mathrm{SSSS}\\ |\,|\,|\,|\end{matrix} + \mathrm{H_2} \rightleftharpoons \begin{matrix}\mathrm{S\square SS}\\ |\,|\,|\,|\end{matrix} + \mathrm{H_2S}.$$

Sulfur anion vacancies have been suggested as catalytic sites for hydrotreatment reactions [26], and it is quite possible that in TPR-S the presence of H_2 in the range of 400–700 K could create such catalytic sites.

Peak 3, between 600 and 1250 K with a maximum at 903 K, is assigned to H_2S (type 4) produced by the reduction of dispersed NiS species and by the reduction of Ni_3S_2 produced by the sintering of the NiMoS phase ($NiMoS \rightarrow Ni_3S_2 + MoS_2$), which is not directly observable under TPR-S conditions [24]. Peak 4, between 700 and 1350 K with a maximum at 1150 K, is ascribed to H_2S (type 4) produced by the reduction of well-dispersed molybdenum species [23,28].

The TPR-S pattern for 0.6NiMo (Fig. 3b) exhibited a similar shape as that observed for NiMo (Fig. 3a). Peaks 1 and 2 did not show any modification compared with the same peaks for the NiMo catalyst. In contrast, peak 3 showed an increased area but a lower maximum reduction temperature (863 K) compared with the equivalent peak for NiMo. These differences suggest an easier reduction, probably due to better dispersion of the nickel species caused by the presence of highly dispersed Ga and to better sulfidation of nickel. The intensity of peak 4 was higher than that measured for the NiMo sample.

The TPR-S pattern for 1.8NiMo (Fig. 3c) did not reveal any important changes over peaks 1 and 2, but the area of the latter was lower by about 7% than that reported for the NiMo solid. Peak 3 exhibited significant differences compared with the NiMo catalyst; a diminution of 80 K over its maximum and an increase in area of ca. 8% was observed. No significant changes were observed for peak 4, except a slight increase of intensity.

The catalyst with the highest amount of Ga (5.9NiMo) showed important differences for the four peaks of NiMo (see Fig. 3d). The highest temperature of peak 1 increased by 10 K compared with peak 1 for the other catalysts, and the area of this peak was slightly higher. Peak 2 showed a significant decrease in area (28%) and a downshift of 20 K, suggesting poor production of H_2S type 2. For peak 3, the highest temperature continued moving down ca. 804 K, and its area was ca. 15% greater than that of NiMo. This modification could be due to the existence of higher amounts of nickel species in the sulfided state over the Ga–Al_2O_3 surface. Peak 4 showed the highest intensity in the patterns of all catalysts, but the maximum temperature also occurred at 1150 K. This increase could be caused by the H_2S produced by the noticeable reduction of gallium due to its high loading in this sample.

3.4. XPS analysis

3.4.1. XPS of Ga–Al_2O_3 support

To investigate the effect of the sulfiding process over gallium and the interaction of this metal with the support, the Ga-containing samples were analyzed by XPS. The samples were β-Ga_2O_3, α-Ga_2S_3 (both commercially supplied), 5.9Ga–Al_2O_3 after calcination, and 5.9GaS–Al_2O_3 sulfided under typical conditions. In the first two cases, the internal reference was the C 1s with binding energy (BE) of 284.5 eV [29] arising from carbon contamination. The BE of Al 2p (74 eV) was used for the other two samples, as explained in the Experimental section.

Regarding the BE for Ga_2O_3, the Ga 3d signal is normally used as a reference because it is the most intense signal. However, a partial overlapping of the Ga 3d signal by the O 2s peak occurs when Ga is supported on alumina, introducing an error in the peak position measurements. Therefore, all of our analyses for gallium-containing samples were performed using the Ga $2p_{3/2}$ level. Table 3 summarizes the BE values for both signals for comparison purposes.

The Ga $2p_{3/2}$ BE (1118.4 ± 0.1 eV) for the bulk-sulfided sample, α-Ga_2S_3, showed a difference of −0.3 eV (±0.2) with respect to that of the oxide sample, β-Ga_2O_3. It is generally accepted that sulfidation of metals produces a slight BE reduction at the same oxidation state. The BE of Ga $2p_{3/2}$ for the calcined 5.9Ga–Al_2O_3 sample showed a difference of about 1.0 eV (±0.2) with respect to that of the sulfided 5.9Ga–Al_2O_3 sample. The BE difference between the oxide- and sulfide-supported samples suggests that at least a fraction of gallium supported on alumina was sulfided, which is consistent with findings of the TPR-S analyses (Table 2). The differences in BE between the bulk and the supported samples suggest that the gallium species on the alumina surface are different from that of the bulk. Therefore, the BE at 1119.5 eV (±0.1) of Ga $2p_{3/2}$ is assigned to the supported $Ga^{3+\delta+}$ species on the calcined material, whereas the value of 1118.7 eV (±0.1) is assigned to the Ga^{3+} species in bulk Ga_2O_3.

3.4.2. XPS of NiMo catalysts

For the NiMo sulfided catalysts with or without Ga, the Mo 3d band is characterized by a doublet with BE (Mo $3d_{5/2}$)

Table 3
Binding energies of catalysts in oxide or sulfide state referenced to Al 2p peak position (74.0 eV). Ga 3d and Ga $3p_{3/2}$ of commercial supplied powders are referenced to carbon peak position (284.5 eV). See comments in the text

Sample code	Treatment	T (K)	Binding energies (eV)				
			Ga 3d	Ga $2p_{3/2}$	Ni $2p_{3/2}$	Mo $3d_{5/2}$	Ni $2p_{3/2}$/Al 2p
NiMo	Sulfidation	673			853.9	228.7	0.039
0.6NiMo	Sulfidation	673	20.0	1118.3	854.1	228.6	0.067
5.9NiMo	Sulfidation	673	19.9	1118.0	853.6	228.3	0.045
5.9Ga–Al_2O_3	Calcination	732	21.1	1119.5			
	Sulfidation	673	20.3	1118.5		–	–
Ga_2O_3	–	–	20.5	1118.7		–	–
Ga_2S_3	–	–	20.2	1118.4		–	–
Ga_2O_3	–	–	20.5[a]			–	–
Ga_2O	–	–	19.0[a]			–	–
Ga	–	–	18.7[a]			–	–

[a] From Ref. [29].

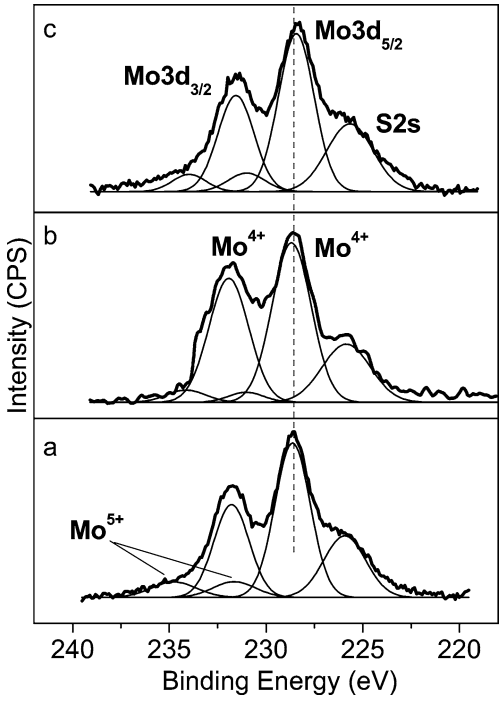

Fig. 4. Comparison of XPS spectra of the Mo 3d and S 2s regions for (a) NiMo, (b) 0.6NiMo, and (c) 5.9NiMo, including curve fitting results.

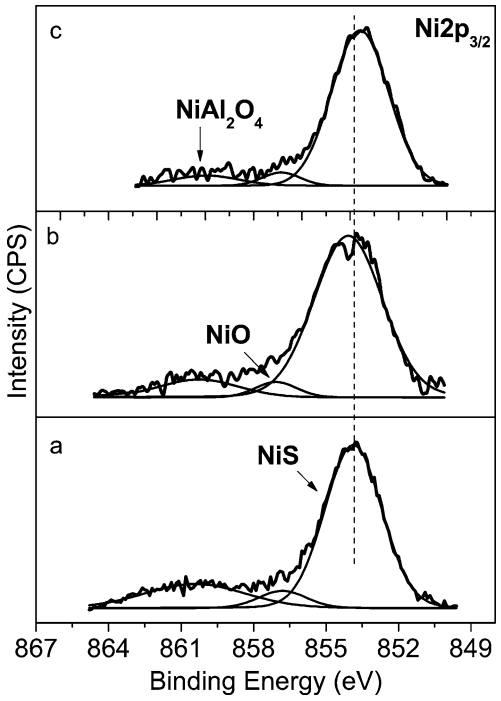

Fig. 5. Comparison of XPS spectra of Ni $2p_{3/2}$ region for (a) NiMo, (b) 0.6NiMo and (c) 5.9NiMo, including curve fitting results.

equals 228.7 eV (±0.1) (Fig. 4) regardless of the Ga presence. The S 2p level for all NiMo catalysts is characterized by a narrow peak with BE 161.6 eV (±0.1), and its position does not change with the amount of Ga. A partial overlapping between S 2p and Ga 3d signals was observed for the sulfided samples, which makes the assessment of the peak position less accurate. The XPS atomic ratios S 2s/Mo 3d were calculated after appropriate deconvolution for all of the NiMo sulfided catalysts, and it was noted that the catalysts with gallium (0.6 and 5.9%) exhibited a significantly higher S 2s/Mo 3d ratio than the NiMo catalyst (results not shown). This excess could be ascribed to the sulfur of gallium sulfide species and to a better sulfidation of the Mo and Ni species.

The XPS spectra of Ni 2p changed its position slightly in the presence of Ga (Fig. 5). The Ni 2p BE shifted upward by 0.2 eV (±0.2) for 0.6NiMo and downward by 0.3 eV (±0.2) for 5.9NiMo with respect to the Ni 2p BE for the reference NiMo catalyst. The deconvolution of the Ni 2p region (Fig. 5) revealed a small peak with BE = 859 eV (±0.1) in all cases. This peak could be assigned to nonsulfided or reduced NiO that could be in the form of $NiAl_2O_4$ [30–32], and the size of this peak decreased when the Ga loading increased. The BE shift of Ni 2p and the size reduction of the peak at 859 eV (±0.1) suggest that some alumina sites that have chemical interactions with nickel, forming $NiAl_2O_4$, could be occupied by gallium species, conducting to a higher concentration of free Ni species that could be more readily sulfided, as discussed earlier for the TPR-S results. The Ni $2p_{3/2}$/Al 2p ratio increased considerably in the presence of Ga (cf. Table 3). Besides, it should be considered that the reduction in BE of the Ni 2p peak could result from a lower proportion of surface Ni species in the "NiMoS" phase. This hypothesis is based on the idea that the electron density

Table 4
Transformation of DBT in a continuous flow reactor, and the deactivation factor observed in the HDS of DBT and 4,6-DMDBT

Catalyst	r_{DBT}	α_T^1	α_T^2
NiMo	6.7	23.6	16.4
0.6NiMo	8.8	9.0	11.4
1.2NiMo	7.4	7.8	9.2
1.8NiMo	6.4	4.3	2.3
2.9NiMo	4.4	1.7	2.9
5.9NiMo	3.2	0.5	2.2

r_{DBT}, transformation rate of DBT (10^{-8} mol s^{-1} g^{-1}). Conversion under 15%.
α_T^1, deactivation factor corresponding to the HDS of DBT (10^{-2} % h^{-1}); (±0.02).
α_T^2, deactivation factor corresponding to the HDS of 4,6-DMDBT (10^{-2} % h^{-1}); (±0.02).

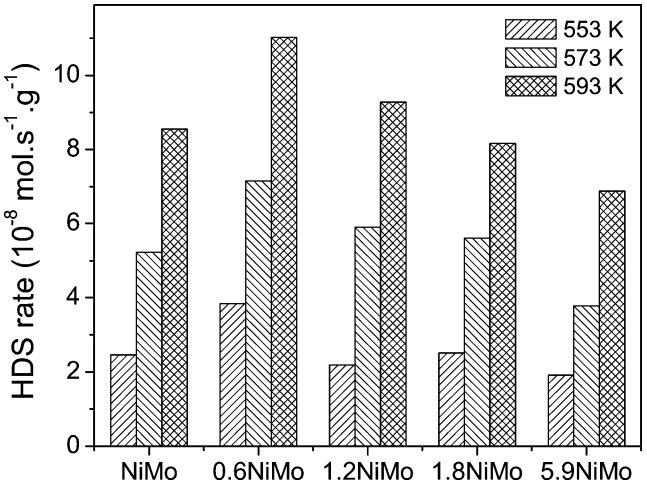

Fig. 6. Transformation of 4,6-DMDBT in a continuous flow reactor at different temperatures.

transfer from Ni to Mo leads to a higher BE of Ni 2p, suggesting a high formal positive charge on Ni atoms [33,34].

3.5. Catalytic tests

3.5.1. HDS of dibenzothiophene

Table 4 gives the results of the DBT transformation rates and reports a deactivation factor to obtain information about the decreased reaction rate with time on stream and thus gain insight into the stability of the samples under these conditions. The deactivation factor (α_T) is expressed in percent per hour and is obtained from the slope of the conversion data plotted versus time when the pseudostationary phase was reached after ca. 5 h on stream. Deactivation was measured after 50 h of reaction. The DBT transformation rates over the 0.6NiMo and 1.2NiMo catalysts were respectively 31 and 10% higher than that of the NiMo sample. However, higher Ga loadings provoked lower catalytic activities than that of the reference solid. In addition, all of the catalysts with gallium exhibited a better stability than the NiMo reference catalyst.

3.5.2. HDS of 4,6-dimethyl-dibenzothiophene

Fig. 6 presents the reaction rates for the HDS of 4,6-DMDBT determined at three different temperatures in the continuous-flow tests of the NiMo catalysts with different amounts of gallium. For all three temperatures, the highest activities were obtained for the 0.6NiMo catalyst and a decrease of activity was observed for higher Ga loadings, following almost the same tendency of the foregoing results exposed for the HDS of DBT. Moreover, the stabilities of the NiMo catalysts with gallium were quite similar to those observed in the HDS of DBT in the continuous flow reactor. The catalysts with the higher gallium amount had the better stability (Table 4).

Table 5
Activities and selectivities for the HDS of 4,6-DMDBT in a batch reactor at 593 K

Catalyst	r_i	r_{DDS}	r_{HYD}	S_{DDS}	S_{HYD}	S_{DDS}/S_{HYD}
NiMo	15	4.4	10.6	29	71	0.40
0.6NiMo	19	6.1	12.9	32	68	0.47
1.2NiMo	17	5.1	11.9	30	70	0.42
1.8NiMo	12	4.3	7.7	36	64	0.56
2.9NiMo	12	4.4	7.6	37	63	0.58
5.9NiMo	9	3.6	6.7	40	60	0.66

r_i, initial transformation rate of 4,6-DMDBT (10^{-8} mol g^{-1} s^{-1}).
r_{DDS}, transformation rate of 4,6-DMDBT through the direct desulfurization pathway (10^{-8} mol $g^{-1}s^{-1}$).
r_{HYD}, transformation rate of 4,6-DMDBT through the hydrogenation pathway (10^{-8} mol g^{-1} s^{-1}).
S_{DDS} and S_{HYD} are, respectively, the initial selectivities of direct desulfurization and hydrogenation pathways (±2), which were estimated by multiplying the initial rate transformation by the corresponding fraction of each pathway.

Table 5 lists the catalytic activities determined for the NiMo catalysts with different loadings of gallium after additional experiments with 4,6-DMDBT in a batch reactor. The catalyst 0.6NiMo was 27% more active than the reference catalyst, and the 1.2NiMo showed an increase of ca. 14%. This enhancing effect disappeared when the amount of gallium was >1.2 wt%; that is, the activity for the (1.8–2.9)NiMo catalysts was 20% lower than that of the NiMo catalyst.

For the most active gallium-containing NiMo catalyst, the increased catalytic activity was reflected to a slightly higher extent over the DDS pathway rate (r_{DDS}) than over the HYD rate (r_{HYD}). The transformation of 4,6-DMDBT through the DDS route (r_{DDS}) was 35 and 16% higher over the 0.6NiMo and 1.2NiMo catalysts, respectively, than over NiMo (Table 5). The transformation of 4,6-DMDBT through the HYD route (r_{HYD}) was 23% higher over the 0.6NiMo and 12% over the 1.2NiMo catalyst. The 1.8NiMo and the 2.9NiMo catalysts had the same r_{DDS} as the NiMo catalyst, whereas the r_{DDS} of the 5.9NiMo catalyst was reduced by 18%. Furthermore, r_{HYD} was more greatly affected by the larger amounts of gallium, with this pathway decreasing by 27% for the 1.8NiMo catalyst, by 28% for the 2.9NiMo catalyst, and by 47% for the 5.9NiMo catalyst. Table 5 summarizes the S_{DDS}/S_{HYD} ratios for all of the

catalysts. From these data, it is difficult to establish a direct correlation between this value and the Ga content in the catalysts.

All HDS tests were performed at different reaction conditions. Based on these results, the enhancing catalytic effect of gallium at low loading over NiMo catalysts activity was confirmed.

4. Discussion

4.1. Effect of gallium over alumina

The textural properties of the unloaded support did not change significantly when gallium was present, probably due to the high dispersion of this metal. XRD did not show any peaks that could suggest the presence of crystals of Ga_2O_3, in agreement with the literature results [19,39]. The XPS analyses showed that the BE values of Ga $2p_{3/2}$ and Ga 3d that we observed and that are described in the literature for bulk compounds (Table 3) are systematically lower than those for the supported gallium species. Although a size effect in XPS has not been reported for metal oxide particles, it has been shown that the development of a TiO_2–SiO_2 interface produced an upshift in the Ti 2p XPS peak and a downshift in the Ti Auger parameter [40]. The values of these shifts in supported gallium oxide indicate changes in the extra-atomic relaxation energy rather than a variation of the initial state [41,42]. In principle, these differences in relaxation could be related to crystal size and/or support effects. As discussed earlier, the gallium is highly dispersed on alumina and this leads to a strong Ga–support interaction. Shimizu et al. [19,43–45] prepared Ga_2O_3/Al_2O_3 and Ga_2O_3/SiO_2 by impregnation with an aqueous solution of $Ga(NO_3)_3$ followed by evaporation and calcination at 873 and 823 K. The X-ray absorption near edge structure (XANES) spectrum showed that the local structure of Ga_2O_3 on SiO_2 was similar to that of octahedral (labeled Ga_o–O) α-Ga_2O_3. The XANES spectrum of Ga_2O_3/Al_2O_3 did not resemble the individual spectra of β- or α-Ga_2O_3, indicating that the Ga ions have a specific local structure as a consequence of the strong interaction with the alumina support showing a tetrahedral coordination (labeled Ga_t–O) [19]. Extended X-ray absorption fine structure (EXAFS) analysis showed that the bond distances of Ga_t–O and Ga_o–O were almost constant for the sample <20 wt% Ga ($R_t = 1.70$ Å and $R_o = 1.95$ Å). These distances are shorter than the bond distances of β-Ga_2O_3 ($R_t = 1.86$ Å and $R_o = 2.02$ Å) and rather close to those of γ-Al_2O_3 ($R_t = 1.72$ Å and $R_o = 1.95$ Å) [44]. These findings and our results suggest that the gallium ions are incorporated in the alumina surface below the monolayer charge (Ga < 20 wt%). This would be quite similar to the model of a surface spinel proposed by Chin and Hercules [46] for Ni/Al_2O_3 and Co/Al_2O_3 systems, in which the surface spinel is formed by diffusion of cations during calcination into the surface cation site of the alumina. In that way, the XPS results are consistent with the literature and indicate a strong interaction between the Ga and the support.

In the TPR-S analyses, H_2S production in all samples suggests that gallium is sulfided under typical sulfiding conditions.

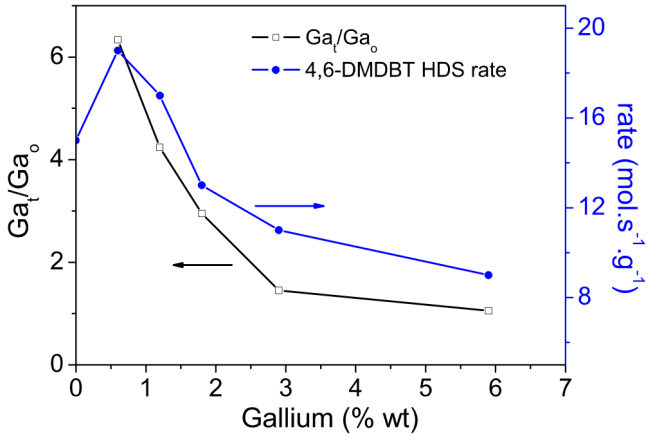

Fig. 7. Evolution of the rate transformation of 4,6-DMDBT as a function of the gallium species. Ga_t, tetrahedrally coordinated; Ga_o, gallium octahedrally coordinated.

This is in agreement with the XPS results showing a downshift in the BE for Ga $2p_{3/2}$ from 1119.5 eV (oxidic state) to 1118.5 eV. The quantitative TPR-S analyses and the elemental sulfur analyses revealed that the Ga sulfidation was incomplete at 673 K, considering that the stoichiometric computations showed a 65% deficit of the expected gallium/sulfur atomic ratio for the five sulfided supports. To verify this finding, we sulfided the 5.9Ga–Al_2O_3 sample at 873 K and found that the quantitative analyses and the sulfur chemical analyses had greater sulfur production than that for the sample 5.9Ga–Al_2O_3 sulfided at 673 K (Table 2). Therefore, under typical sulfiding conditions, some part of Ga remained in the oxidic state.

In the TPR-S patterns of the supports (Ga–Al_2O_3), H_2S production occurred in two different zones (Fig. 2). The difference of temperature (ΔT) between the two more intense peaks in each zone was ca. 600 K. This is three times larger that the ΔT between the peaks observed in the reduction of Ga_2S_3 (bulk), where the ΔT between the adjacent peaks was about 160 K (see Fig. 1). Hence, for the supported gallium samples, neither the H_2S produced in zone I nor the H_2S produced in zone II can be assigned to a consecutive reduction similar to that occurring in the unsupported samples. It can be suggested that each reduction zone corresponds to a different species of gallium supported on alumina. Hence, in the TPR-S, the production of H_2S at low Ga content (zone I) can be assigned to the tetrahedral species (Ga_t) and zone II, which started to be more intense at high Ga content, can be assigned to the octahedral species (Ga_o) (Fig. 7). Therefore, the ratio of Ga_t/Ga_o decreased as the Ga loading increased. This is in agreement with the results of Shimizu et al. [43–45].

4.2. Effect of gallium on the NiMo/γ-Al_2O_3 catalysts

The more remarkable features of the NiMo TPR-S are as follows:

1. The type 2 and type 3 H_2S, produced between 300 and 900 K (peak 2), presented the same intensity and area under the curve for the catalysts with low Ga content; whereas

this production was reduced for the catalysts with a higher Ga content.
2. The H_2S assigned to the reduction of NiS and Ni_3S_2 (produced by the sintering of the NiMoS phase) showed a downshift in its maximum temperature and an increase in its area in the presence of gallium. These differences suggest an easier reduction of the nickel species.

Regarding the XPS results, the main effect of Ga was on the BE of Ni 2p. The BE of Ni 2p was 853.9 eV for the NiMo catalyst supported over alumina and 854.1 eV for the 0.6NiMo catalyst; the ΔBE between the NiMo reference and the 5.9NiMo catalyst was 0.3 eV. For both catalysts, it has been proposed that Co (Ni) ions supported on alumina could be present as diluted $NiAl_2O_4$ species in tetrahedral coordination [46] and on the surface of the support as a $NiAl_2O_4$-like phase in mainly octahedral coordination [27,47]. It has been suggested that the subsurface $NiAl_2O_4$ species are not sulfidable, whereas the surface $NiAl_2O_4$-like species are partially sulfidable at 673 K [24]. Therefore, a fraction of Ni was not sulfided, and, consequently, these nickel species do not participate in the HDS activity.

Bearing in mind the TPR-S results, the XPS results could have two explanations:

1. The addition of small amounts of gallium could result in an interaction with tetrahedral sites (as discussed earlier), leading to an increase in the free nickel species. This suggests that more Ni participates in the NiMoS phase and in free Ni as NiS, although these two phases could have opposite effects on the BE of Ni 2p. In other words, if the amount of NiS species increased on the surface of the alumina, then a downshift in BE would be observed, as has been shown previously [48], but an increase in the Ni species that participate in the NiMoS phase could result in an upshift in BE of the Ni 2p, due to the charge transfer of Ni to the MoS_2 slabs [26]. The catalytic results support this latter idea, as discussed later in the paper.
2. The addition of relatively high amounts of Ga could result in the interaction of gallium with both tetrahedral and octahedral sites, leading to a dramatic increase in the octahedrally surrounded Ni ions. At the same time, the promoter (Ni) may not be well associated with the molybdenum (MoS_2) due to a negative effect of the octahedral gallium on the dispersion of the MoS_2. When the amount of Ga increases, the tetrahedral Al^{3+} neighboring sites starts to be covered by gallium, and, consequently, Ga particle size increases, leading to the formation of octahedral gallium species.

As discussed earlier, Ga interacts mainly with the tetrahedral sites of alumina at low loadings. MoO_3 also interacts with these sites [48]. In this work, XPS analysis reveals a diminution of the Mo^{5+} species (Fig. 4) between the reference and the 0.6NiMo catalyst, suggesting a better sulfidation of MoO_3. Therefore, the presence of Ga at low loadings seems to be positive for the HDS properties, considering the high activity for the NiMo catalysts. In the case of high Ga loading, a downshift in the BE (0.4 ± 0.2 eV) was observed in the Mo 3d level. This suggests that Ga at low loadings increases the sulfidation of MoO_3, although high Ga loadings could negatively affect the dispersion of MoO_3. Clearly, the increased amount of sulfidable Ni species cannot compensate for the decrease of MoO_3 dispersion. No clear relationship can be established between our XPS results and the dispersion of Mo, because of the interference of gallium (mainly at high loadings) over the atomic ratio of Mo 3d/Al 2p.

4.3. Gallium effect on the NiMo catalyst activity

As noted earlier, small amounts of gallium enhanced the activity of the NiMo catalyst in the HDS of DBT and 4,6-DMDBT by about 30% for the 0.6NiMo and 15% for the 1.2NiMo. This enhancement is most likely due to the occupation of the tetrahedral sites by gallium, resulting in an increase in the amount of nickel species that can participate in the MoS_2 decoration. A similar effect has been observed from adding small amounts of Zn [6,11–13] or Mg [6–9] to the alumina before the impregnation of Mo and Ni (Co). These metals (Me) can form species like $MeAl_2O_4$, which decrease the inactive $NiAl_2O_4$ species and consequently increase the HDS activity. Moreover, the results shown in Fig. 7 correlate the HDS activity with the gallium species present in the catalytic surface detected by TPR-S. The maximum activity is reached when the gallium species in the catalysts are mainly tetrahedral (Ga_t). When the octahedral gallium species (Ga_o) start to increase, the activity of the catalysts decreases in almost a parallel manner with the decreasing Ga_t/Ga_o ratio, implying that the gallium effect is no longer positive at relatively high amounts ($\geqslant$1.8 wt%).

For the 0.6NiMo catalyst, the transformation of the 4,6-DMDBT through the DDS was 35% higher than that over the reference catalyst, and the r_{HYD} was 23% higher than that of the NiMo catalyst. These results indicate an increase in MoS_2 slab promotion, in agreement with the XPS results for the 0.6NiMo catalyst. Furthermore, some results in the literature suggest that better promotion is reflected mainly in the transformation of 4,6-DMDBT through the DDS pathway [49]. For the 1.2NiMo catalysts, the r_{DDS} increases about 16% compared with the NiMo catalysts, whereas the r_{HYD} was 12% higher. This implies less MoS_2 promotion than in the 0.6NiMo catalyst but more MoS_2 promotion than in the NiMo catalyst. In contrast, when the amount of gallium was increased, both pathways started to decrease, although the r_{HYD} was affected more significantly than the r_{DDS}. Considering the XPS results for the 5.9NiMo catalyst, we suggest that, in contrast to the NiMo, 0.6NiMo, and 1.2NiMo catalysts, the NiMoS phase is poorly formulated, leading to a change in selectivity approaching that of the MoS_2/Al_2O_3 catalysts, as reported previously [38].

Therefore, we can propose that the promoter (Ni) is better associated with the molybdenum (MoS_2), creating more NiMoS phase, whereas at the same time that the S anions are slightly more basic, provoking a better C–S bond cleavage when the amount of Ga is $<$1.2 wt%.

5. Conclusions

We have found that small amounts of Ga (e.g., 0.6 and 1.2 wt%) had a positive effect and induced increased activity of a typical NiMo supported over gamma alumina without modifying its initial textural properties. XPS and TPR-S analyses indicated the existence of more sulfidable, well-dispersed Ni species participating in the decoration of the NiMoS phase, leading to increased HDS activity. This effect might be caused by the existence of gallium in tetrahedral coordination over the alumina sites, which enhances the sulfidability of MoO_3 and decreases the formation of $NiAl_2O_4$ in tetrahedral coordination.

Acknowledgments

This research was performed under the auspices of the Institut de Recherches sur la Catalyse, Instituto Mexicano del Petróleo, and CONACYT (Project 42204-Y). E. Altamirano is grateful to the Postgraduate Cooperation Program (PCP France–Mexico) and to CONACyT for a graduate scholarship.

References

[1] H. Topsøe, B.S. Clausen, Catal. Rev.-Sci. Eng. 26 (1984) 395.
[2] P. Ratnasamy, S. Sivasanker, Catal. Rev.-Sci. Eng. 22 (1980) 401.
[3] X. Carrier, J.F. Lambert, M. Che, J. Am. Chem. Soc. 119 (1997) 10137.
[4] N.Y. Topsøe, H. Topsøe, J. Catal. 84 (1983) 386.
[5] N.P. Martinez, P.C.H. Mitchell, in: H.F. Barry, P.C.H. Mitchell (Eds.), Proceedings of the 3rd Climax International Conference on the Chemistry and Uses of Molybdenum, Climax Molybdenum, Ann Arbor, MI, 1979, p. 105.
[6] G. Muralidhar, F.E. Massoth, J. Shabtai, J. Catal. 85 (1984) 44.
[7] F. M Mulcahy, M. Houalla, D.M. Hercules, J. Catal. 139 (1993) 72.
[8] A.R. Saini, B.G. Johnson, F.E. Massoth, Appl. Catal. 40 (1988) 157.
[9] K. Jirátová, M. Kraus, Appl. Catal. 27 (1986) 21.
[10] A. Cimino, M. Lo Jacono, M. Schiavello, J. Phys. Chem. 79 (1975) 243.
[11] C.L. Kibby, H.E. Swift, J. Catal. 45 (1976) 231.
[12] V.H.J. De Beer, T.H.M. Van Sint Fiet, G.H.A.M. Van Der Steen, A.C. Zwaga, G.C.A. Schuit, J. Catal. 35 (1974) 297.
[13] B.R. Strohmeier, D.M. Hercules, J. Catal. 86 (1984) 266.
[14] M. Lo Jacono, M. Schiavello, V.H.J. De Beer, G. Minelli, J. Phys. Chem. 81 (1977) 16.
[15] Y.C. Park, H.K. Rhee, Appl. Catal. A 179 (1999) 145.
[16] T. Olorunyolemi, R. Kydd, J. Catal. 158 (1996) 583.
[17] D. Zuo, M. Vrinat, H. Nie, F. Maugé, Y. Shi, M. Lacroix, D. Li, Catal. Today 93–95 (2004) 751.
[18] F. Labruyère, M. Lacroix, D. Schweich, M. Breysse, J. Catal. 167 (1997) 464.
[19] K. Nishi, K. Shimizu, M. Takamatsu, H. Yoshida, A. Satsuma, T. Tanaka, S. Yoshida, T. Hattori, J. Phys. Chem. B 102 (1998) 10190.
[20] J.C. Hutter, in: P. Pascal, A. Chrétieu, Y. Trambouze, J.C. Hutter, W. Freundlich (Eds.), Nouveau traité de chimie minérale, vol. IV, Masson et compagnie, Paris, 1961, p. 669.
[21] N.K. Nag, D. Frankel, J.A. Moulijn, B.C. Gates, J. Catal. 66 (1980) 162.
[22] P. Arnoldy, J.A.M. van den Heijkant, G.D. de Bok, J.A. Moulijn, J. Catal. 92 (1985) 35.
[23] B. Scheffer, N.J.J. Dekker, P.J. Mangnus, J.A. Moulijn, J. Catal. 121 (1990) 31.
[24] P.J. Mangnus, A. Bos, J.A. Moulijn, J. Catal. 146 (1994) 437.
[25] P.J. Mangnus, A. Riezebos, A.D. van Langeveld, J.A. Moulijn, J. Catal. 151 (1995) 178.
[26] H. Topsøe, B.S. Clausen, F.E. Massoth, in: J.R. Anderson, M. Boudart (Eds.), Hydrotreating Catalysis Science and Technology, Springer, Berlin, 1996.
[27] B. Scheffer, P. Molhoek, J.A. Moulijn, Appl. Catal. 46 (1989) 11.
[28] L. Qu, W. Zhang, P.J. Kooyman, R. Prins, J. Catal. 215 (2003) 7.
[29] A.M. Venezia, Catal. Today 77 (2003) 359.
[30] U.S. Ozkan, L. Zhang, S. Ni, E. Moctezuma, J. Catal. 148 (1994) 181.
[31] K.T. Ng, D.M. Hercules, J. Phys. Chem. 80 (1976) 2094.
[32] Y.J. Huang, J.A. Schwarz, Appl. Catal. 36 (1988) 163.
[33] A.N. Startsev, Catal. Rev.-Sci. Eng. 37 (1995) 353.
[34] A.P. Shepelin, P.A. Zhdan, V.A. Burmistrov, A.N. Startsev, Yu.I. Yermakov, Appl. Catal. 11 (1984) 29.
[35] M. Houalla, N.K. Nag, A.V. Sapre, D.H. Broderick, B.C. Gates, AIChE J. 24 (1978) 1015.
[36] V. Meille, E. Schulz, M. Lemaire, M. Vrinat, J. Catal. 170 (1997) 29.
[37] T. Isoda, S. Nagao, X. Ma, Y. Korai, I. Mochida, Appl. Catal. A 150 (1997) 1.
[38] M. Egorova, R. Prins, J. Catal. 225 (2004) 417.
[39] M.P. Pardo, M. Guittard, A. Chilouet, A. Tomas, J. Solid State Chem. 102 (1993) 423.
[40] S.E. Collins, M.A. Baltanás, J.L. Fierro, A.L. Bonivardi, J. Catal. 211 (2002) 252.
[41] C.D. Wagner, Faraday Discuss. Chem. Soc. 60 (1975) 291.
[42] C.D. Wagner, A. Joshi, J. Electron. Spectrosc. Relat. Phenom. 47 (1988) 283.
[43] K. Shimizu, M. Takamatsu, K. Nishi, H. Yoshida, A. Satsuma, T. Hattori, Chem. Commun. (1996) 1827.
[44] K. Shimizu, M. Takamatsu, K. Nishi, H. Yoshida, A. Satsuma, T. Tanaka, S. Yoshida, T. Hattori, J. Phys. Chem. B 103 (1999) 1542.
[45] K. Shimizu, A. Satsuma, T. Hattori, Appl. Catal. B 16 (1998) 319.
[46] R.L. Chin, D.M. Hercules, J. Phys. Chem. 86 (1982) 360.
[47] S. Kasztelan, J. Grimblot, J.P. Bonelle, J. Phys. Chem. 91 (1987) 1503.
[48] A.N. Startsev, A.V. Kalinkin, I.I. Zakharov, D.G. Aksenov, V.N.J. Parmon, J. Mol. Catal. A 151 (2000) 171.
[49] D. Zuo, D. Li, H. Nie, Y. Shi, M. Lacroix, M. Vrinat, J. Mol. Catal. A 211 (2004) 179.